Available online at www.sciencedirect.com
SCIENCE DIRECT
International Journal of Heat and Fluid Flow 27 (2006) 424–435
International Journal of HEAT AND FLUID FLOW
www.elsevier.com/locate/ijhff

A comparative study of numerical models for Eulerian–Lagrangian simulations of turbulent evaporating sprays

D.I. Kolaitis, M.A. Founti *

Heterogeneous Mixtures and Combustion Systems, Thermal Engineering Department, School of Mechanical Engineering, National Technical University of Athens, Heroon Polytechniou 9, Polytechnioupoli Zografou, 15780 Athens, Greece

Received 3 August 2004; received in revised form 8 November 2005; accepted 13 January 2006
Available online 9 March 2006

Abstract

The paper comparatively assesses the computational performance of a selected number of theoretical and semi-empirical liquid droplet evaporation models that focus on thermodynamic non-equilibrium effects, physical property estimation methods and convective and blowing effect corrections for the calculation of the heat and mass transfer rates. Three different test cases are examined in order to establish the most appropriate model, in terms of both physical accuracy and numerical efficiency for implementation in two-phase CFD spray simulations. The considered cases span from a single, isolated droplet, evaporating in a convective environment, to a fully turbulent, evaporating, hollow cone spray; for the latter case, an in-house Eulerian–Lagrangian CFD code is used. Predictions are validated against experimental data for all test cases and the most promising model is established on the basis of accuracy and CPU time requirements. As a result, the "infinite conductivity" equilibrium droplet evaporation model, combined with an analytic expression for the convective and blowing effect correction can be proposed as most appropriate for CFD spray applications.

Keywords: Spray modelling; Droplet evaporation; Heat and mass transfer; Two-phase CFD

1. Introduction

Liquid droplets, in a form of a spray, are employed in a wide spectrum of industrial applications. Oil fired furnaces and boilers, internal combustion engines and gas turbines utilize liquid fuel sprays in order to accelerate the rates of evaporation and combustion by increasing the free fuel surface area. The fuel is usually injected into the combustion chamber through an atomizing nozzle, resulting in the production of a spray comprising a large number of droplets, typically the order of 10–100 μm in diameter. Spray combustion involves a variety of complex phenomena, such as simultaneous momentum, mass and energy transfer as well as oxidative chemical reactions, which usually take place in a fully turbulent environment.

Numerical simulation of droplet dynamics and heat and mass transfer processes in a turbulent, two-phase flow is a particularly challenging problem. Phenomena such as primary and secondary atomization, droplet evaporation, turbulent dispersion, droplet collisions and splashing must be modelled in order to accurately describe the two-phase flowfield. Momentum, mass and energy interchange between the gas and liquid phases are crucial for the accurate prediction of the interacting droplet evaporation phenomena that are addressed in a number of review papers (Law, 1982; Faeth, 1983; Aggarwal et al., 1984; Sirignano, 1993; Miller et al., 1998). Experimental investigations (Ranz and Marshall, 1952; Kulmala et al., 1995) and single-droplet computational fluid dynamics (CFD) simulations (Renksizbulut and Haywood, 1988; Abramzon and Sirignano, 1989; Haywood et al., 1989; Chiang et al., 1992) have yielded correlations that can be used for numerical modelling of turbulent sprays.

* Corresponding author. Tel.: +30 210 7723605; fax: +30 210 7723527.
E-mail address: mfou@central.ntua.gr (M.A. Founti).

0142-727X/$ - see front matter © 2006 Elsevier Inc. All rights reserved.
doi:10.1016/j.ijheatfluidflow.2006.01.002

Nomenclature

B_M	Spalding mass transfer number
B_T	Spalding heat transfer number
C_p	constant pressure specific heat [J kg^{-1} K^{-1}]
D_{AB}	binary mass diffusion coefficient [m^2 s^{-1}]
D	droplet diameter [m]
F	correction factor
k	thermal conductivity [W m^{-1} K^{-1}]
L	fuel's latent heat of evaporation [J kg^{-1}]
L_K	Knudsen layer thickness [m]
Le	Lewis number
$\dot{m}$	droplet mass evaporation rate [kg s^{-1}]
m_d	droplet mass [kg]
MW	molecular weight [kg kmol^{-1}]
Nu	Nusselt number
p	pressure [Pa]
Pr	Prandtl number
$\overline{R}$	universal gas constant [J kmol^{-1} K^{-1}]
Re_d	droplet Reynolds number
Sc	Schmidt number
Sh	Sherwood number
t	time [s]
T	temperature [K]
$\vec{u}$	velocity vector [m s^{-1}]
Y	fuel vapour mass fraction

Greeks

β	evaporation parameter
μ	dynamic viscosity [Pa s]
ρ	density [kg m^{-3}]
χ	fuel vapour mole fraction

Subscripts

BP	boiling point
d	droplet
G	gas phase
L	liquid phase
m	average gas–vapour "film" conditions
neq	non-equilibrium
ref	reference value
s	droplet surface
v	fuel vapour
0	non-modified quantities, initial conditions
∞	"free-stream" conditions

The current energy crisis emphasizes once more the need for design and performance optimization of oil-fuelled combustion devices, in particular in view of the potentials of mineral fuel substitution by alternatives, e.g. biofuels. The required detailed thermo-kinetic modelling of liquid fuel evaporation and combustion (e.g. through implementation of chemical kinetic mechanisms for multi-component fuels) imposes high computational costs, in terms of CPU time requirements. Thus, it becomes of paramount importance to have in hand accurate, flexible and especially low computational cost droplet evaporation models that can be reliably implemented in complex CFD approaches. The paper aims to provide the reader with an overview of the most important thermo-fluid mechanisms occurring in single droplet and spray evaporation and at the same time highlight criteria for appropriate model choice for CFD applications. For this reason, the work evaluates a wide range of sub-grid droplet evaporation models, used to describe non-equilibrium effects, thermo-physical properties, convective and blowing effects. The assessed models are among those commonly incorporated in commercial CFD codes. Low evaporation rate, atmospheric pressure conditions are considered here, as typical cases that can be used for the development of detailed thermo-kinetic mechanisms and of multi-component or low-grade liquid fuel combustion.

The comparison and evaluation of the considered models is performed following a two-stage procedure. At first, the ability of the selected models to accurately describe the temporal diameter evolution of single isolated droplets, evaporating in a constant temperature and constant velocity environment is assessed by comparison with two different experimental datasets. In the second stage, an in-house two-phase Eulerian–Lagrangian CFD code is used in order to simulate a confined, atmospheric pressure, turbulent, evaporating spray test case. Predictions of droplet diameter, velocity and mass flux spatial evolution are compared with experimental data and the suitability and performance of each model for implementation in a two-phase CFD code are evaluated in terms of both physical accuracy and numerical efficiency.

2. Single droplet evaporation modelling

Contemporary analytical research on droplet evaporation uses a bottom-up approach that fabricates idealized configurations leading to a simplified model that breaks down a complex problem into a number of idealized, isolated sub-problems. These sub-system level descriptions examine specific features related to environmental, property and operational factors, as well as the nature of droplet dynamics and energetic coupling of interior and exterior fields. A representative selection of such idealized sub-models, aimed to relax a number of physical assumptions employed in the "standard" droplet evaporation model, is examined in this study.

2.1. "Standard" droplet evaporation model

In the "standard" model, proposed by Godsave (1953) and Spalding (1953), an algebraic equation is used to estimate the mass evaporation rate of a single, isolated droplet, evaporating in an infinite, constant temperature and constant velocity air environment. Phase equilibrium at the droplet's surface is assumed; therefore, the Clausius–Clapeyron equation can be used in order to calculate the surface mole fraction of the fuel vapour. A series of plausible assumptions, such as spherical symmetry, isolated droplet, quasi-steady gas-phase flow and single fuel species, were made to formulate the original model. The relative performance of various models, which have been proposed in the literature to relax further assumptions, such as uniform and constant droplet temperature (fixed at the wet-bulb value), phase equilibrium at the droplet surface (fuel vapour at saturation pressure that corresponds to the respective droplet surface temperature) and omission of vapour blowing effects, are evaluated.

It has been recognized that transient droplet heating phenomena have a significant effect on the evaporation process (Law, 1982; Faeth, 1983). As a result, the evaporation rate equation should be coupled with a time-dependent energy equation. There are two main approaches to describe liquid-phase transport phenomena inside the droplet. In the first case, known as the "infinite conductivity model", "rapid mixing" conditions are assumed, signifying that the droplet temperature varies with time but is spatially uniform. In the second case, the "finite conduction" model assumes that heat is transferred within the liquid solely by thermal diffusion, resulting in the emergence of a distinct temperature profile across the droplet radius. These approaches are usually considered as the two extremes bounding the possible range of real conditions. Several investigators have not observed significant improvements when implementing the "finite conduction" model in comparison to the "infinite conductivity model" (Law, 1982; Aggarwal et al., 1984; Berlemont et al., 1991; Chen et al., 1997; Miller et al., 1998; Tolpadi et al., 2000). For this reason, the latter is used in the current comparative study. The "standard" droplet evaporation model serves as a "basis" for the testing and evaluation of the considered sub-models.

2.2. Non-equilibrium effects

Bellan and Harstad (1987), proposed an evaporation model, which takes into consideration the non-equilibrium phenomena that may appear in the gas–droplet interface. The model incorporates the non-equilibrium Langmuir–Knudsen law through the definition of a non-equilibrium vapour mole fraction at the droplet surface (Miller et al., 1998). The main equations used in the "standard" equilibrium (E1) and non-equilibrium (E2) sub-grid droplet evaporation models are presented in Table 1.

2.3. Estimation of physical properties

An important parameter affecting the predictive capabilities of droplet evaporation models is the reliability of the procedure for computing the physical properties of the gas (and to a lesser extend of the liquid) phase (Gouesbet and Berlemont, 1999). Empirical correlations for the properties of pure substances are broadly available (e.g. Reid et al., 1987); however, a "mixing rule" is needed for the "film" boundary layer region, developing on the outer side of the droplet and consisting of air and fuel vapour. For the estimation of the "film" temperature and vapour mass fraction reference values, the "1/3 rule" is known to yield the most reliable results (Hubbard et al., 1975; Yuen and Chen, 1976). According to the "1/3 rule", the droplet surface conditions are considered to be dominating in the "film" region, by a factor of 2, over the "far field" conditions. Three different physical properties estimation methods are comparatively evaluated here, namely the "ideal gas standard additive rules", the Wilke (1950) mixing rule and the Herning and Zipperer (1936) approximation. They are presented (M1–M3) in Table 2.

Table 1
Equilibrium and non-equilibrium droplet evaporation models

Abb.	Equations	Reference
E1	$\dot{m} = \pi D \rho_m D_{AB} Sh \ln(1 + B_M),\ m_d C_{p,L} \frac{dT_d}{dt} = \pi D Nu k_m (T_\infty - T_d) - \dot{m} L$	Spalding (1953)
E2	$\chi_{s,neq} = \chi_s - \frac{2 L_K \beta}{D},\ L_K = \frac{\rho_G D_{AB} k_G}{\mu_G C_{p,G}} \left(\frac{2\pi T_d \bar{R}}{MW_L}\right)^{1/2},\ \beta = \frac{C_{p,G}\dot{m}}{2\pi k_G D}$	Bellan and Harstad (1987)

Table 2
Estimation methods for evaporation "film" physical properties

Abb.	Equations	Reference
M1	$\Phi_m = Y_{ref}\Phi_v + (1 - Y_{ref})\Phi_G$	Reid et al. (1987)
M2	$\Phi_m = \frac{\chi_{ref}\Phi_v}{\chi_{ref} + (1-\chi_{ref})\Omega_{vG}} + \frac{(1-\chi_{ref})\Phi_G}{\chi_{ref}\Omega_{Gv} + (1-\chi_{ref})},\ \Omega_{vG} = \frac{[1+(\Phi_v/\Phi_G)^{1/2}(MW_G/MW_v)^{1/4}]^2}{[8(1+MW_v/MW_G)]^{1/2}}$	Wilke (1950)
M3	$\Omega_{vG} = \left(\frac{MW_G}{MW_v}\right)^{1/2} = \frac{1}{\Omega_{Gv}}$	Herning and Zipperer (1936)

2.4. Convective correlations

In practical spray conditions, soon after the injection of the droplet in the hot gas stream, the external flow is "adjusted" to the presence of the droplets. Due to the relative "slip velocity" between the droplet and the gas, heat and mass boundary layers are developed near the droplet surface. The gas-phase convective environment has a considerable impact on the droplet evaporation process; both heat- and mass-transfer rates between the gas and liquid phases are enhanced, whereas at the same time, liquid circulation is generated inside the droplet, due to the shear stress at the gas/liquid interface, leading to an increase in the liquid-phase transfer rates. In order to consider these phenomena, the diffusive mass flux and energy transfer equations, are "corrected" by implementing semi-empirical correlations for the calculation of both mass (Sh) and heat transfer (Nu) non-dimensional numbers in the case of forced convection. A characteristic selection of semi-empirical convective correlations available in the literature is considered here.

One of the first and most reliable convective droplet evaporation correlations was that of Froessling (1938). The original correlation has been later modified by Ranz and Marshall (1952) and Gnielinski (1975), by altering the value of the 0.552 arithmetic constant (0.6 and 0.664, respectively). However, for low evaporation rate conditions, Kolaitis and Founti (2002) established that the differences among the various modified correlations are negligible. The Kulmala et al. (1995) correlation is essentially a variation of the Froessling correlation, which has been derived from experimental data regarding water evaporation in an air environment, taking into account the explicit temperature dependence of the mass diffusion coefficient. Clift et al. (1978), proposed a correlation that utilizes a parameter varying with Re_d, assuming a value of unity for the Stokes flow regime ($Re_d < 1$). Finally, in the correlation of Faeth and Lazar (1971), a multiplicative correction for heat and mass transfer is introduced in the original Froessling correlation. The investigated convective correlations appear (C1–C4) in Table 3. Own numerical experiments agreed with the observations of Sirignano (1993) that predictions are improved when the definition of the droplet Reynolds number is based on the free-stream density and the average gas film viscosity.

2.5. Blowing effect correlations

The "standard" evaporation model does not take into account the effects inflicted on the evaporation process by the generated fuel vapour that is moving in the outward direction. Surface blowing results in the thickening of both heat and mass boundary layers, thus impeding transport phenomena near the droplet surface. The streaming vapour leaving the droplet surface is heated in the thermal boundary layer until it reaches the ambient temperature at the edge of it. The energy absorbed by this superheating process is actually subtracted from the potential energy that can reach the liquid surface, thus the heat transfer rate is further hindered. In order to take account the aforementioned phenomena, different correlations, of varying complexity, have been proposed. The examined Stefan flow correlations (B1–B4) are presented in Table 4.

An analytic expression deduced from the solution of the gas-field equations near the droplet surface, utilizing the quasi-steady flow assumption, appears in the textbook of

Table 3
Convective correlations for mass and heat transfer calculations

Abb.	Equations	Reference
C1	$Sh = 2 + 0.552 Re_d^{1/2} Sc^{1/3}$	Froessling (1938)
C2	$Sh = 2.009 + 0.514 Re_d^{1/2} Sc^{1/3}$	Kulmala et al. (1995)
C3	$Sh = 1 + (1 + Re_d Sc)^{1/3} f(Re_d), f(Re_d) = \begin{cases} 1, & 0 < Re_d < 1 \\ Re_d^{0.077}, & 1 < Re_d < 400 \end{cases}$	Clift et al. (1978)
C4	$Sh = 2 + 0.552 Re_d^{1/2} Sc^{1/3} \left(1 + \frac{1.232}{Re_d Sc^{4/3}}\right)^{-1/2}$	Faeth and Lazar (1971)

Table 4
Blowing effect correlations for mass and heat transfer calculations

Abb.	Equations	Reference
B1	$Nu = Nu_0 \left(\frac{\beta}{e^{\beta}-1}\right)$	Bird et al. (1960)
B2	$Sh = 2 + \frac{Sh_0 - 2}{F_M}$, $F_M = (1 + B_M)^{0.7} \frac{\ln(1+B_M)}{B_M}$, $B_T = (1 + B_M)^{\Phi} - 1$, $\Phi = \left(\frac{C_{p,v}}{C_{p,G}}\right)\left(\frac{Sh}{Nu}\right)\frac{1}{Le}$, $m_d C_{p,L} \frac{dT_d}{dt} = \dot{m}\left(\frac{C_{p,v}(T_\infty - T_d)}{B_T} - L\right)$	Abramzon and Sirignano (1989)
B3	$Sh = \frac{2+0.87 Re_d^{1/2} Sc^{1/3}}{(1+B_M)^{0.7}}$, $Nu = \frac{2+0.57 Re_d^{1/2} Pr^{1/3}}{(1+B_T)^{0.7}}$, $B_T = \frac{C_{p,G}(T_\infty - T_d)}{L}$	Haywood et al. (1989)
B4	$Sh = \frac{2+0.39 Re_R^{0.54} Sc^{0.76}}{(1+B_M)^{0.557}}$, $Nu = \frac{2+0.454 Re_R^{0.615} Pr^{0.98}}{(1+B_T)^{0.7}}$, $Re_R = \frac{\rho_\infty (\vec{u}_G - \vec{u}_d) D}{2\mu_m}$	Chiang et al. (1992)

Bird et al. (1960). The expression considers the impact of surface blowing on the heat transfer rate by introducing a modified Nusselt number in the droplet energy conservation equation. The non-modified *Nu* number is determined using one of the available semi-empirical convection correlations (Section 2.4).

A number of numerical studies, based on the solution of the full Navier–Stokes equations for both the liquid and the gas phase have been conducted by various research groups (Abramzon and Sirignano, 1989; Haywood et al., 1989; Chiang et al., 1992). Such detailed calculations, apart from providing useful insight regarding the occurring momentum, mass and heat transport phenomena, produce simplified models that can be used in complex spray simulations, where the computational cost becomes a decisive parameter. In the extensively used model of Abramzon and Sirignano (1989), two correction factors are introduced, representing the relative change of the thermal and diffusional film thicknesses due to Stefan flow, in order to calculate the modified *Nu* and *Sh* numbers, respectively. However, to determine the value of the heat transfer correction factor, an iterative procedure is needed. It should be noted that Abramzon and Sirignano (1989) also suggested the use of an alternative form for the droplet's energy equation. Haywood et al. (1989) proposed a different set of heat and mass transfer correlations, for droplet evaporation at moderate temperature and atmospheric pressure conditions. In this case, no iterative calculation procedure is required, since the non-dimensional heat transfer number is straightforwardly calculated. The computational results of Chiang et al. (1992), pertaining to higher evaporation rate conditions, that are more characteristic of practical combustion systems, yielded a similar set of correlations. In this case, the mean Reynolds number is calculated by utilizing the value of the droplet radius.

3. Two-phase flow numerical modelling

The two-phase CFD code used to simulate the gas/droplet flowfield of a turbulent, evaporating spray is the in-house developed 2PHASE code. The code is based on a Eulerian–Lagrangian computational formulation for the continuous and dispersed phase respectively. It has been previously validated and satisfactorily evaluated in a number of test cases (Klipfel et al., 1998; Founti and Klipfel, 1998; Kolaitis and Founti, 2005) regarding gas–particle, liquid–particle and gas–liquid flows.

3.1. Continuous phase

The continuous phase is treated as a steady, incompressible, turbulent flow and is computed by solving the Reynolds-averaged Navier–Stokes equations. The ensuing system of mass, momentum, species and energy conservation equations is solved via a finite volume method based on a staggered grid arrangement, using the SIMPLE algorithm and a hybrid differencing discretization scheme (Patankar, 1980). Turbulence quantities are modelled using the modified version of the k–ε turbulence model, proposed by Sung et al. (1990), which takes into account the radius of curvature of the flow. The model has proved to yield better prediction accuracy with low computational cost compared to the standard k–ε model in recirculating flows with abrupt area changes (Founti and Klipfel, 1998). Standard wall functions are used for the near-wall boundary conditions; convective heat transfer phenomena are also taken into account (Kader and Yaglom, 1972).

3.2. Dispersed phase

The Lagrangian approach is utilized for the calculation of the dispersed phase. A multitude of computational "parcels", each one representing a "group" of real droplets that have the same properties (diameter, velocity and temperature), is traced through the flowfield. Each parcel's trajectory is calculated by solving the instantaneous droplet motion equations in a three-dimensional Cartesian frame of coordinates (in order to avoid the singularity that droplet radial position may assume by applying cylindrical coordinates), with the use of a fourth order Runge–Kutta method. The forces that are taken into account are the drag force (using the well-known Schiller and Nauman (1933) correlation to calculate the droplet's drag coefficient), the pressure gradient force and the gravitational force. The large droplet-to-gas density ratio (ρ_d/ρ_G) in the case studied indicates that the effects of the added mass, shear lift and the Basset history forces are negligible and can be neglected (Faeth, 1983; Maxey and Riley, 1983; Crowe et al., 1998; Sommerfeld, 1998; Brandon and Aggarwal, 2001).

Phase coupling between the gas and the droplets is achieved by calculating source/sink terms for the interfacial mass, momentum, species concentration, thermal and turbulent energy exchange (two-way coupling), following a modified version (Sommerfeld, 1998) of the PSI-cell approach of Crowe et al. (1977). Droplet evaporation phenomena are taken into account by solving the droplet mass and energy balance equations for every Lagrangian time-step. The temporary local droplet diameter and temperature values are updated, while at the same time and for the specific computational cell that the droplet resides, heat "sink" and mass "source" terms are calculated and stored, in order to be used in the subsequent two-way coupling iteration. The computational time-step used for the droplet evaporation calculations is determined dynamically and is a fraction of the respective Lagrangian step, since a finer time scale is usually needed in order to resolve the numerically stiff droplet energy equation.

A major parameter affecting spray evolution characteristics is the interaction between droplets and gas-phase turbulence. Droplet turbulent dispersion is modelled using a modified version (Sommerfeld et al., 1992) of the Lagrangian stochastic separated flow (SSF) model of Gosman and Ioannides (1983) by sampling random Gaussian gas veloc-

ity fluctuations and accounting for the crossing trajectories and eddy dissipation effects. There are numerous reports in the literature, suggesting that when axisymmetric simulations are employed, an artificial accumulation in mass-flux predictions at the centreline is emerging (MacInnes and Bracco, 1992; Chen and Pereira, 1996; Sommerfeld, 1998; Loth, 2000). To resolve this problem a "drift correction" term, proposed by Sommerfeld et al. (1993a), is applied to the turbulent dispersion model.

4. Simulation results

Three different experimental datasets, pertaining to low pressure, low evaporation rate conditions, are utilized for the evaluation and comparison of the considered models. The first and second test cases refer to a single isolated droplet, evaporating in a constant temperature and constant velocity air environment and are used to evaluate the predictive capabilities of the various models. In the third test case, a fully turbulent spray, evaporating in an open-flowing experimental set-up is considered to validate the implementation of the best performing models in a two-phase CFD code, in terms of both physical accuracy and numerical efficiency. For the single droplet evaporation cases (Test cases 1 and 2), only the droplet mass and energy conservation differential equations are solved, whereas the two-phase CFD code is used for the numerical simulation of the fully turbulent evaporating spray (Test case 3). In order to elucidate the effect of each individual model on the computational results, a variety of "model combinations" is examined. Each "model combination" comprises three different sub-models, regarding the non-equilibrium phenomena (models E1 and E2), the physical properties estimation method (M1–M3) and either the convective (C1–C4) or blowing effect (B1–B4) correlations (the latter inherently encompass the gas convection effects). A straightforward naming convention is followed; for instance, the "model combination" E1M2C1 stands for the "standard"-equilibrium evaporation model (E1), utilizing the Wilke mixing rule (M2) and the Froessling convection correlation (C1).

4.1. Test case 1: hexane single droplet evaporation

In the first test case, based on the measurements of Downing (1966), a hexane droplet of initial diameter $D_0 = 1.76$ mm and initial temperature $T_{d,0} = 281$ K was exposed to a continuous flowing air stream of constant velocity ($u_\infty = 1.584$ m/s). The air temperature ($T_\infty = 437$ K) was kept constant at a level moderately higher than the liquid's boiling point ($T_{BP} = 344.6$ K). An overall comparison between experimental data and computational predictions for the temporal evolution of the droplet's squared diameter, utilizing all the considered model combinations, is presented in Fig. 1. In Fig. 1a, the effect of the non-equilibrium phenomena is investigated, by implementing models E1 and E2, while keeping the same mixing rule (M3) and blowing effect correction (B1). In both cases the predictions are identical, indicating that non-equilibrium effects have no discernible impact in the considered low evaporation rate conditions. This observation is in agreement with previous studies (Miller et al., 1998; Kolaitis and Founti, 2003), where it is reported that non-equilibrium effects become important either at very intense evaporation rate

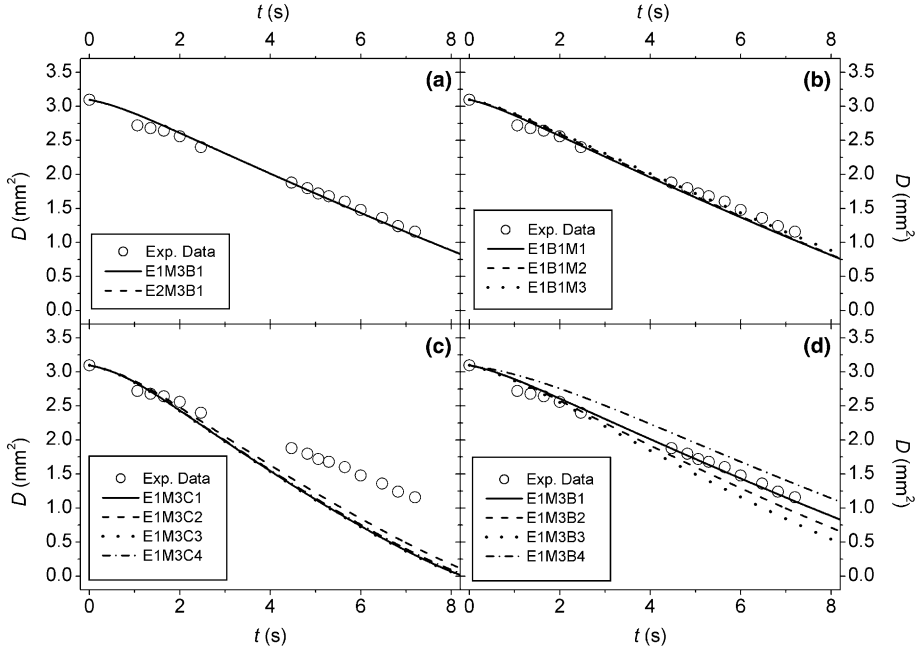

Fig. 1. Experimental data and predictions for the temporal evolution of a hexane droplet's squared diameter (Test case 1). Effects of (a) non-equilibrium phenomena, (b) mixing rule, (c) convective correlation and (d) blowing effect correlation.

conditions or when small initial droplet sizes (<50 μm) are encountered. Concerning the physical properties estimation method, Fig. 1b reveals that the differences among the various models predictions are insignificant; only M3 exhibits a slightly better performance than M1 and M2.

In Fig. 1c, predictions utilizing the various convective corrections (C1–C4) are compared to the experimental data. Although all computational results lie close to each other, significant discrepancies are observed with respect to the measurements, especially in the region of $t > 3$ s. The failure of all convective correlations to follow the experimental trends is attributed to the significance of the Stefan flow effects; the agreement is significantly improved when the blowing effect corrections are utilized (Fig. 1d). Evidently, predictions utilizing corrections B1–B4 outperform those using correlations C1–C4; this observation suggests that in order to achieve accurate droplet evaporation predictions, it is necessary to take account of the Stefan flow effects, even in low pressure, low evaporation conditions. However, there are still differences among the various blowing effect corrections. When model B3 is used, a high evaporation rate is predicted and droplet evaporation time is underpredicted, when compared to results with B2 and B4 that lie on either side of the experimental data. Predictions utilizing model B1 agree with the experimental values better than any other model, rendering it the model of choice for implementation into a CFD code.

The temporal evolution of the calculated *Nu* number, shown in Fig. 2, indicates notable differences among the predictions with the different convection (C1–C4) and blowing effect (B1–B4) correlations. All predictions using the convection corrections are almost identical. However, predictions utilizing the blowing effect corrections significantly diverge from each other. Models B3 and B4 follow a slightly decreasing trend, similar to the trend observed in predictions using models C1–C4, although the predicted absolute values of the *Nu* number are remarkably different. Such behaviour can be attributed to the similar form of the respective correlations. On the other hand, the exponential nature of models B1 and B2, results in a totally different behaviour. The sudden drop in *Nu* values during the initial evaporation stage (up to 2 s) is followed by a nearly constant, slightly decreasing region. There are no available experimental data to validate the *Nu* number predictions. However, the respective droplet diameter predictions presented in Fig. 1d suggest that models B1 and B2 are closer to the experimentally determined trends.

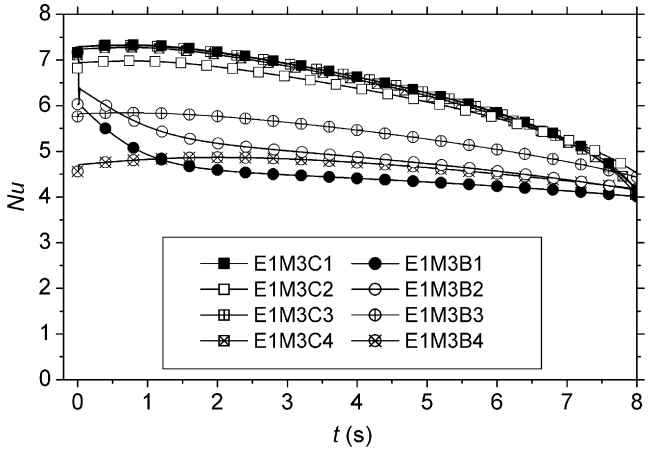

Fig. 2. Calculated Nusselt number temporal evolution (Test case 1).

4.2. Test case 2: heptane single droplet evaporation

The second test case examined refers to a heptane droplet ($D_0 = 1.052$ mm, $T_{d,0} = 300$ K) suspended on a permanent holder fixed inside a thermal wind tunnel. The time evolution of the droplet diameter was recorded by Daif et al. (1999) utilizing a CCD camera, for the case of a constant velocity and temperature ($u_\infty = 3.2$ m/s, $T_\infty = 356$ K) air stream, under low evaporation rate conditions ($T_{BP} = 371.6$ K). Measured and predicted values for the temporal evolution of the droplet's squared diameter are depicted in Fig. 3. Once more (Fig. 3a), thermodynamic non-equilibrium effects are negligible in the considered low evaporation rate conditions. Fig. 3b, reveals that the original Wilke mixing rule (M2) yields identical results with the Herning and Zipperer approximation (M3), while both outperform the ideal gas standard additive rules (M1). Predictions using the convective corrections (C1–C4) exhibit discrepancies when compared to the measurements, although all models perform sufficiently well during the initial evaporation period (up to 1.5 s). The implementation of the blowing effect corrections (B1–B4) results in a clear improvement in prediction accuracy. Models B1 and B2 lie very close to the experimental data; the performance of the former is slightly better than the latter.

In conclusion, it has been established that for a low pressure, low evaporation rate environment, non-equilibrium phenomena (E2) do not have a significant effect in the droplet evaporation history. Regarding the physical properties estimation method, slight improvements are observed when the M3 mixing rule is used. Models that take into account only gas convection effects (C1–C4) are not sufficient to accurately predict droplet evaporation rates; simulation results are clearly improved when Stefan flow effects are additionally considered (B1–B4). Among the various blowing effect corrections, model B1 clearly exhibits the best performance, yielding very reasonable results when compared to experimental data.

4.3. Test case 3: isopropyl alcohol turbulent evaporating spray

As a further evaluation step, the most promising models are implemented in the two-phase CFD code in order to validate their predictive capabilities in an actual turbulent evaporating spray simulation case. Both equilibrium (E1) and non-equilibrium (E2) evaporation models are tested, whereas only the most accurate mixing rules (M2 and

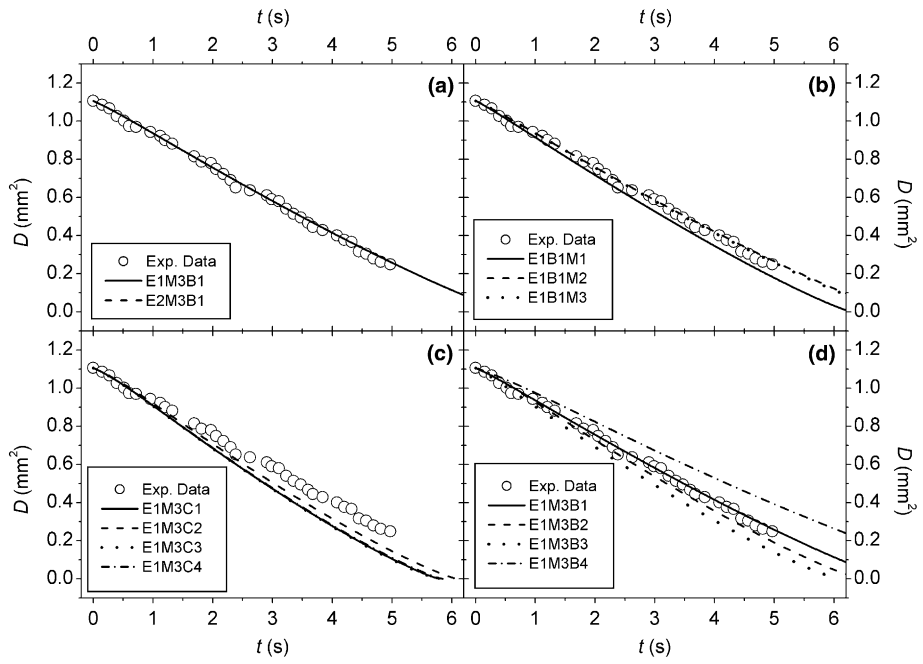

Fig. 3. Experimental data and predictions for the temporal evolution of a heptane droplet's squared diameter (Test case 2). Effects of (a) non-equilibrium phenomena, (b) mixing rule, (c) convective correlation and (d) blowing effect correlation.

M3) are taken into account. The blowing effect corrections exhibiting the best results (B1 and B2) are also considered.

Detailed experiments providing comprehensive information regarding the droplet characteristics (velocity, diameter and flow rate) close to the injection point are very scarce since it is difficult to perform accurate measurements very close to the atomizing nozzle. The experimental data of Sommerfeld and Qiu (1998), referring to an atmospheric pressure isopropyl alcohol ($T_{BP} = 355.45$ K) spray have been extensively used in numerous evaporating spray CFD simulations (Sommerfeld et al., 1993b; Chen and Pereira, 1995; Chen and Pereira, 1998; Sommerfeld, 1998; Naud, 2003). The test case refers to a downward flowing spray, at a temperature of 313 K (created via a commercial Simplex hollow cone nozzle) enclosed by a 200 mm diameter cylindrical test section. The co-flowing turbulent air stream, preheated at 373 K, was simultaneously blown through a concentric annulus of 40 mm inner and 64 mm outer diameter. The void fraction of the flow was calculated to be 99.998%, thus classifying the spray as a dilute two-phase flow.

The computational domain, measuring 1.0 m axially $\times$ 0.1 m radially, is discretized using 131×70 non-uniform, cylindrically axisymmetric, rectangular grid nodes. The grid is refined close to the nozzle tip to improve local flow resolution. Computational results utilizing this grid arrangement do not deviate more than 1.5% when compared to those obtained by using a grid with 183×125 nodes, thus ensuring grid independence. The available phase Doppler anemometry measurements regarded the radial profiles of droplet velocity, diameter and mass flux for seven downstream axial positions. The experimental data obtained 3 mm downstream the atomizing nozzle are used as inlet conditions for the Lagrangian simulations; the remaining data are used for the validation of the numerical results. The droplets are injected from 10 discrete starting locations along the nozzle, matching exactly the corresponding "PDA measuring points" of Sommerfeld and Qiu (1998). A total number of 100,000 droplet "parcels" are injected and tracked throughout the flowfield, for 30 two-way coupling iteration cycles, in order to keep statistical fluctuations associated with stochastic particle tracking at an acceptable level.

In Fig. 4, predictions for the radial distribution of the main droplet properties, using four different evaporation model combinations, are compared to the experimental data, at six different axial positions. The "best performing" model combination (E1M3B1), proposed by the single droplet evaporation evaluation tests, consists of the thermodynamic equilibrium evaporation model (E1), utilizing the Herning and Zipperer (1936) approximation (M3) and the Bird et al. (1960) blowing effect correction (B1). Effects of the non-equilibrium phenomena (E2M3B1), the physical property evaluation method (E1M2B1) and the blowing effect correction (E1M3B2) are also investigated. All model combinations show very good agreement with the measurements. Droplet mean axial velocity and liquid mass flux predictions are practically insensitive to the model combinations tested, as also previously observed (Aggarwal and Chitre, 1991; Chen and Pereira, 1996).

In general, droplet mean axial velocities become more uniform with increasing distance from the nozzle since large droplets, exhibiting initially higher slip velocities, decelerate more rapidly than small droplets due to the

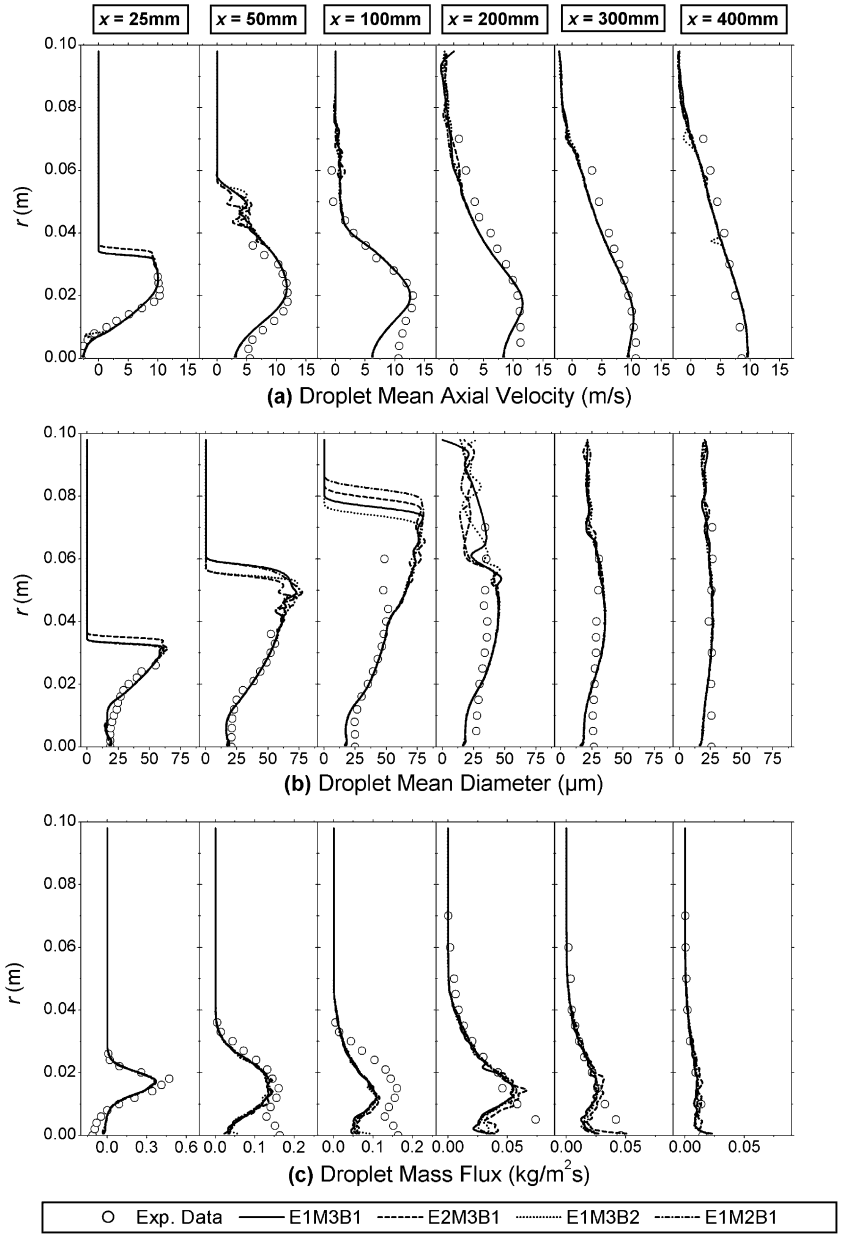

Fig. 4. Test case 3: Experimental data and predictions for (a) droplet mean axial velocity, (b) droplet mean diameter and (c) droplet liquid mass flux radial profiles.

non-linear nature of the drag law. All model combination predictions lie very close to the droplet mean axial velocity measurements (Fig. 4a), with the exception of the region near the symmetry axis, at the 100 mm and 200 mm axial positions; similar discrepancies have been also observed by Sommerfeld (1998).

The observed diameter evolution behaviour (Fig. 4b) is typical of hollow cone sprays: the mean droplet diameter is generally increasing with the radial distance from the symmetry axis. Moreover, evaporation and turbulent dispersion phenomena result in the "flattening" of the diameter profile downstream the atomizing nozzle, leading to a radially uniform droplet size distribution. The droplet mean diameter prediction discrepancies near the spray's edge are similar to those observed by Sommerfeld et al. (1993b), Chen (1994), Chen and Pereira (1996), who attributed this behaviour to the small number of computational parcels moving at this region. These discrepancies give rise to significant compromises in the accuracy of the statistical weighting procedure.

A satisfying agreement with experimental data is observed in Fig. 4c, where liquid mass flux predictions are presented. The observed discrepancies near the symmetry axis are in line with similar observations of Chen and Pereira (1995) and Naud (2003). These discrepancies are attributed to the well-known issue of unrealistic accumulation of droplet mass flux near the centre-line (Chen and Pereira, 1996; Sommerfeld, 1998), which has been partially

remedied by the implementation of a drift-correction term in the droplet turbulent dispersion model of Sommerfeld et al. (1993a). In any case, as experimental data suggest, moving downstream the injection plane, the bulk of the droplet mass flux is moving towards the centre, due to the annular air jet entrainment.

4.4. Computational requirements

In two-phase CFD spray simulations, a multitude of droplets are tracked through the flowfield for a number of two-way coupling iterations. As a result, droplet evaporation calculations that are performed for every Lagrangian time-step and for each computational parcel impose a significant computational cost to the entire calculation procedure. Consequently, it is important to evaluate the numerical efficiency of the various models, apart from their physical accuracy. The subject of computational requirements has not been given proper attention in previous comparative studies of sub-grid evaporation models, both for single droplet and full spray CFD simulations.

Average values are calculated after recording the CPU-time consumption for 10 consecutive "runs" of every model combination. Fig. 5 compares CPU-time requirements for the three test cases examined; the results are normalized by the least computational intensive combination (E1M1C1). The differences among computational requirements of the various models are more pronounced in the single evaporating droplet test cases than in the two-phase CFD case, since the latter simulations involve the calculation of numerous physical phenomena apart from droplet evaporation. However, a consistent trend is observed for all test cases.

In comparison with the "standard" thermodynamic equilibrium evaporation model (E1M3B1), an additional computational cost of the order of approximately 7% is inflicted in the single droplet cases, when the effects of the non-equilibrium phenomena are taken into account (E2M3B1). The full spray simulations exhibit higher CPU-time requirements by 1%, but since no apparent improvements are observed after the implementation of the E2 model (Figs. 1a, 3a and 4), the "standard" equilibrium model (E1) is proposed as adequate for low evaporation rate simulations.

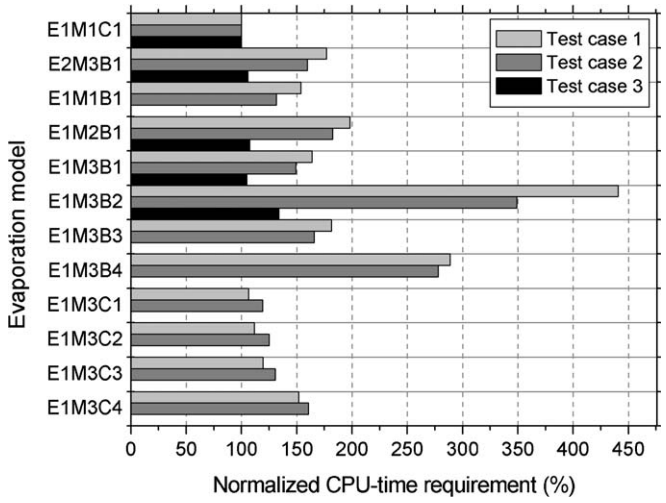

Fig. 5. Normalized CPU-time requirements for the various model combinations.

Regarding the physical properties evaluation method, the more accurate Wilke mixing rule (E1M2B1) requires 29–39% more time than the standard ideal gas additive rules (E1M1B1). However, the Herning and Zipperer approximation (E1M3B1) that produces identical results with the Wilke rule (Figs. 1b and 3b), needs only 4–7% more time than the E1M1B1 combination. In the full spray simulations, the difference between sub-models M2 and M3 is 2.4% in favour of the latter. Therefore, model M3 is proposed as more economic.

The required extra computational cost (when compared to the "reference" combination E1M1C1) of the various convective correlations (C1–C4) ranges from 6.5% to 60.5%. However, since these correlations have proved to be insufficient (Fig. 1c), blowing effects should be taken into account. The 49–64% additional time needed, when the B1 model is utilized, is essential in order to achieve better prediction quality. It is quite remarkable though, that while the B1 model exhibits the best "physical" performance among the blowing effect corrections (Figs. 1d and 3d), it is, at the same time, the least computationally intensive. Compared to B1, the other blowing effect corrections require additional computational resources ranging from approximately 11% (B3) to 76–86% (B4) and even 134–169% (B2). In the two-phase simulations, where only the "best" performing models are compared, model B1 requires 28% less CPU-time than the B2 model, since the latter utilizes a sophisticated and numerically complex iterative procedure in order to calculate the heat transfer correction term. Therefore, the conclusions of the single droplet evaporation modelling analysis are further supported, towards the selection of B1. It should be noted here that this correction is very scarcely used in Lagrangian droplet evaporation simulations (Berlemont et al., 1991; Miller and Bellan, 1999).

5. Concluding remarks

A broad combination of models, capable of simulating the variety of heat and mass transfer phenomena emerging during liquid droplet evaporation, were comparatively assessed, in terms of physical accuracy and numerical effectiveness, in three test cases, referring to low pressure, low evaporation rate conditions.

The "standard" equilibrium droplet evaporation model, utilizing the "infinite liquid conductivity" assumption, served as a basis for the investigation of a number of sub-models accounting for non-equilibrium effects, physical property estimation methods and convective and blowing effect corrections. It was shown, against comparison

with single droplet evaporation experimental data, that for low evaporation rate conditions, thermodynamic non-equilibrium effects have no influence on droplet evaporation characteristics. The Herning and Zipperer model exhibited the best performance among the various "mixing rules" utilized to calculate the physical properties of the gas "film" surrounding the droplet. Corrections that account only for gas convection effects were found to be insufficient to effectively describe the temporal evolution of the droplet diameter in the considered test cases. Predictions were significantly improved when blowing effect phenomena were taken into account. Among the four different "Stefan flow" corrections examined, an analytic expression, deduced from the solution of the gas-field equations near the droplet surface, exhibited the best performance in all the considered test cases. The numerical efficiency of the various models was examined by recording the computational resources requirements. The results of the CPU-time requirement comparison further supported the conclusions drawn from the physical accuracy evaluation procedure.

In order to evaluate the implementation of the examined models in actual multi-droplet gas–liquid simulations, a Eulerian–Lagrangian two-phase CFD code was used for the simulation of an atmospheric pressure, fully turbulent, evaporating, hollow cone spray configuration. In this case, all model combinations demonstrated a similar predictive behaviour and all the respective predictions agreed reasonably well with the experimental data. The CPU-time consumption comparison, revealed on one hand similar trends with the single droplet cases, even though the observed relative differences were significantly smaller, due to the multitude of complex interacting phenomena involved in the CFD simulations.

Acknowledgements

The present study has been financially supported by the EC in the frame of an EU-project (contract no. ENK6-CT-2000-00317).

References

Abramzon, B., Sirignano, W.A., 1989. Droplet vaporization model for spray combustion calculations. Int. J. Heat Mass Transfer 32, 1605–1618.

Aggarwal, S.K., Chitre, S., 1991. Computation of turbulent evaporating sprays. J. Propulsion Power 7, 213–220.

Aggarwal, S.K., Tong, A.Y., Sirignano, W.A., 1984. A comparison of vaporization models in spray calculations. AIAA J. 22, 1448–1457.

Bellan, J., Harstad, K., 1987. Analysis of the convective evaporation of nondilute clusters of drops. Int. J. Heat Mass Transfer 30, 125–136.

Berlemont, A., Grancher, M.S., Gouesbet, G., 1991. On the Lagrangian simulation of turbulence influence on droplet evaporation. Int. J. Heat Mass Transfer 34, 2805–2812.

Bird, R.B., Steward, W.E., Lightfoot, E.N., 1960. Transport Phenomena. Wiley, New York, 636-684.

Brandon, D.J., Aggarwal, S.K., 2001. A numerical investigation of particle deposition on a square cylinder placed in a channel flow. Aerosol Sci. Technol. 34, 340–352.

Chen, G., Aggarwal, S.K., Jackson, T.A., Switzer, G.L., 1997. Experimental study of pure and multicomponent fuel droplet evaporation in a heated air flow. Atomizat. Sprays 7, 317–337.

Chen, X.Q., 1994. Numerical simulation of steady and unsteady two-phase spray flows. Ph.D. thesis. Instituto Superior Tecnico – Lisbon, Portugal.

Chen, X.Q., Pereira, J.C.F., 1995. Prediction of evaporating spray in anisotropically turbulent gas flow. Numer. Heat Transfer: Part A 27, 143–162.

Chen, X.Q., Pereira, J.C.F., 1996. Computation of turbulent evaporating sprays with well-specified measurements: a sensitivity study on droplet properties. Int. J. Heat Mass Transfer 39, 441–454.

Chen, X.Q., Pereira, J.C.F., 1998. Numerical study of the effects of gas temperature fluctuation on a turbulent evaporating spray. Atomizat. Sprays 8, 63–82.

Chiang, C.H., Raju, M.S., Sirignano, W.A., 1992. Numerical analysis of convecting, vaporizing fuel droplet with variable properties. Int. J. Heat Mass Transfer 35, 1307–1324.

Clift, R., Grace, J.R., Weber, M.E., 1978. Bubbles, Drops and Particles. Academic Press, New York.

Crowe, C.T., Sharma, M.P., Stock, D.E., 1977. The particle-source-in-cell (PSI-cell) model for gas–droplet flows. J. Fluids Eng. 99, 325–332.

Crowe, C., Sommerfeld, M., Tsuji, Y., 1998. Multiphase Flows with Droplets and Particles. CRC Press, Boca Raton, pp. 57–112.

Daif, A., Bouaziz, M., Chesneau, X., Cherif, A.A., 1999. Comparison of multicomponent fuel droplet vaporization experiments in forced convection with the Sirignano model. Exp. Thermal Fluid Sci. 18, 282–290.

Downing, C.G., 1966. The evaporation of drops of pure liquids at elevated temperatures: rates of evaporation and wet-bulb temperatures. AIChE J. 12, 760–766.

Faeth, G.M., 1983. Evaporation and combustion of sprays. Prog. Energy Combust. Sci. 9, 1–76.

Faeth, G.M., Lazar, R.S., 1971. Fuel droplet burning rates in a combustion gas environment. AIAA J. 9, 2165–2171.

Founti, M., Klipfel, A., 1998. Experimental and computational investigations of nearly dense two-phase sudden expansion flows. Exp. Thermal Fluid Sci. 17, 27–36.

Froessling, N., 1938. Ueber die Verdunstung fallender Tropfen. Gerlands Beitraege zur Geophysik 52, 170–216.

Gnielinski, V., 1975. Berechnung mittlerer Warme-und Stoffübergangskoeffizienten an laminar und turbulent überströmten Einzelkörpern mit Hilfe einer einheitlichen Gleichung. Forsch. Ing.-Wes. 41, 145–153.

Godsave, G.A.E., 1953. Studies of the combustion of drops in a fuel spray: studies of the combustion of drops in a fuel spray: the burning of single drops of fuel. In: Proceedings of the Combustion Institute, vol. 4, pp. 818–830.

Gosman, A.D., Ioannides, E., 1983. Aspects of computer simulation of liquid fueled combustor. J. Energy 7, 482–490.

Gouesbet, G., Berlemont, A., 1999. Eulerian and Lagrangian approaches for predicting the behaviour of discrete particles in turbulent flows. Prog. Energy Combust. Sci. 25, 133–159.

Haywood, R.J., Nafziger, R., Renksizbulut, M., 1989. A detailed examination of gas and liquid phase transient processes in convective droplet evaporation. J. Heat Transfer 111, 495–502.

Herning, F., Zipperer, L., 1936. Beitrag zur Berechnung der Zaehigkeit technischer Gasgemische aus den Zaehigkeitswerten der Einzelbestandteile. Gas- und Wasserfach 79, 49–69.

Hubbard, G.E., Denny, V.E., Mills, A.F., 1975. Droplet evaporation: effects of transients and variable properties. Int. J. Heat Mass Transfer 18, 1003–1008.

Kader, B.A., Yaglom, A.M., 1972. Heat and mass transfer laws for fully turbulent wall flows. Int. J. Heat Mass Transfer 15, 2329–2351.

Klipfel, A., Founti, M., Zaehringer, K., Martin, J.P., Petit, J.P., 1998. Numerical simulation and experimental validation of the turbulent combustion and perlite expansion processes in an industrial perlite expansion furnace. Flow, Turb. Combust. 60, 283–300.

Kolaitis, D., Founti, M., 2002. Comparing evaporation rates of single suspended droplets. In: Proceedings of the Tenth Workshop on Two-Phase Flow Predictions, Merseburg, Germany, pp. 72–81.

Kolaitis, D., Founti, M., 2003. Scrutinizing evaporation models for computational modelling of turbulent sprays. In: Proceedings of the Ninth International Conference on Liquid Atomization and Spray Systems (ICLASS 2003), Sorrento, Italy, Paper 2–18.

Kolaitis, D., Founti, M., 2005. Numerical simulation of diesel spray evaporation exploiting the "stabilized cool flame" phenomenon. Atomizat. Sprays 15, 1–18.

Kulmala, M., Vesala, T., Schwarz, J., Smolik, J., 1995. Mass transfer from a drop. II. Theoretical analysis of temperature dependent mass flux correlation. Int. J. Heat Mass Transfer 38, 1705–1708.

Law, C.K., 1982. Recent advances in droplet vaporization and combustion. Progr. Energy Combust. Sci. 8, 171–201.

Loth, E., 2000. Numerical approaches for motion of dispersed particles, droplets and bubbles. Progr. Energy Combust. Sci. 26, 161–223.

MacInnes, J.M., Bracco, F.V., 1992. Stochastic particle dispersion modeling and the tracer-particle limit. Phys. Fluids A 4, 2809–2824.

Maxey, R.M., Riley, J.J., 1983. Equation of motion for a small rigid sphere in a non-uniform flow. Phys. Fluids 25, 883–889.

Miller, R.S., Bellan, J., 1999. Direct numerical simulation of a confined three-dimensional gas mixing layer with one evaporating hydrocarbon-droplet-laden stream. J. Fluid Mech. 384, 293–338.

Miller, R.S., Harstad, K., Bellan, J., 1998. Evaluation of equilibrium and non-equilibrium evaporation models for many-droplet gas–liquid flow simulations. Int. J. Multiphase Flow 24, 1025–1055.

Naud, B., 2003. PDF modeling of turbulent sprays and flames using a particle stochastic approach. Ph.D. thesis. Technische Universiteit Delft, The Netherlands.

Patankar, S.V., 1980. Numerical Heat Transfer and Fluid Flow. Hemisphere, New York, pp. 79–138.

Ranz, W.E., Marshall, W.R., 1952. Evaporation from drops: I. Chem. Eng. Prog. 48, 141–146.

Reid, R.C., Prausnitz, J.M., Poling, B.E., 1987. The Properties of Gases and Liquids, fourth ed. McGraw-Hill, Singapore, pp. 404–417.

Renksizbulut, M., Haywood, R.J., 1988. Transient droplet evaporation with variable properties and internal circulation at intermediate Reynolds numbers. Int. J. Multiphase Flow 14, 189–202.

Schiller, L., Nauman, A., 1933. Ueber die grundlegende Berechnung bei der Schwerkraftaufbereitung. Ver. Deutsch. Ing. 44, 318–320.

Sirignano, W.A., 1993. Fluid dynamics of sprays – 1992 Freeman scholar lecture. J. Fluids Eng. 115, 345–378.

Sommerfeld, M., 1998. Analysis of isothermal and evaporating turbulent sprays by phase-Doppler anemometry and numerical calculations. Int. J. Heat Fluid Flow 19, 173–186.

Sommerfeld, M., Qiu, H.H., 1998. Experimental studies of spray evaporation in turbulent flow. Int. J. Heat Fluid Flow 19, 10–22.

Sommerfeld, M., Ando, A., Wennerberg, D., 1992. Swirling, particle-laden flows through a pipe expansion. J. Fluids Eng. 114, 648–656.

Sommerfeld, M., Kohnen, G., Rueger, M., 1993a. Some open questions and inconsistencies of Lagrangian particle dispersion models. In: Proceedings of the Ninth Symposium on Turbulent Shear Flows, Kyoto, Japan, Paper 15.1.

Sommerfeld, M., Kohnen, G., Qiu, H.H., 1993b. Spray evaporation in turbulent flow: numerical calculations and detailed experiments by phase-Doppler anemometry. Revue de l' Institut Francais du Petrole 48, 677–695.

Spalding, D.B., 1953. The combustion of liquid fuels. In: Proceedings of the Combustion Institute 4, pp. 847–864.

Sung, H.J., Jang, H.C., Cho, C.H., 1990. Curvature-dependent two-equation model for recirculating flows. In: Proceedings of Engineering Turbulence Modelling and Experiments. Elsevier Science Publishing Co., pp. 33–42.

Tolpadi, A.K., Aggarwal, S.K., Mongia, H.C., 2000. An advanced spray model for application to the prediction of gas turbine combustor flow fields. Numer. Heat Transfer A 38, 325–340.

Wilke, C.R., 1950. A viscosity equation for gas mixtures. J. Chem. Phys. 18, 517–519.

Yuen, M.C., Chen, L.W., 1976. On drag of evaporating liquid droplets. Combust. Sci. Technol. 14, 147–154.